(4) Verdier, P. H. *J. Chem. Phys.* **1966**, *45*, 2118.
(5) Monnerie, L.; Gény, F. *J. Chim. Phys.* **1969**, *66*, 1961. Gény, F.; Monnerie, L. *Ibid.* **1969**, *66*, 1708. Gény, F.; Monnerie, L. *J. Polym. Sci., Polym. Phys. Ed.* **1979**, *17*, 131, 147.
(6) Helfand, E. *J. Chem. Phys.* **1978**, *69*, 1010. Helfand, E.; Wasserman, Z.; Weber, T. A. *Macromolecules* **1980**, *13*, 526.
(7) Hall, C. K.; Helfand, E. *J. Chem. Phys.* **1982**, *77*, 3275.
(8) Helfand, E. *J. Chem. Phys.* **1971**, *54*, 4651.
(9) Skolnick, J., Helfand, E. *J. Chem. Phys.* **1980**, *72*, 5489. Helfand, E.; Skolnick, J. *J. Chem. Phys.* **1982**, *77*, 5714.
(10) Orwoll, R. A.; Stockmayer, W. H. *Adv. Chem. Phys.* **1969**, *15*, 305.
(11) Valeur, B.; Jarry, J. P.; Gény, F.; Monnerie, L. *J. Polym. Sci., Polym. Phys. Ed.* **1975**, *13*, 667, 675, 2251.
(12) Jones, A. A.; Stockmayer, W. H. *J. Polym. Sci., Polym. Phys. Ed.* **1977**, *15*, 847.
(13) Boyer, R. F. *Rubber Chem. Technol.* **1963**, *34*, 1303. Schatzki, T. F. *J. Polym. Sci.* **1962**, *57*, 496; *Polym. Prepr. (Am. Chem. Soc., Div. Polym. Chem.)* **1965**, *6*(2), 646.
(14) Baysal, B.; Lowry, B. A.; Yu, H.; Stockmayer, W. H. In *Dielectric Properties of Polymers*; Karasz, F. E., Ed.; Plenum: New York, 1972; p 329.
(15) Stockmayer, W. H. *Pure Appl. Chem.* **1966**, *15*, 539.
(16) Matsuo, K.; Kuhlmann, K. F.; Yang, W. H.; Gény, F.; Stockmayer, W. H.; Jones, A. A. *J. Polym. Sci, Polym. Phys. Ed.* **1977**, *15*, 1347.
(17) Kramers, H. A. *Physica* **1940**, *7*, 284.
(18) Glauber, R. S. *J. Math. Phys.* **1963**, *4*, 294.
(19) Anderson, J. E. *J. Chem. Phys.* **1970**, *52*, 2821.
(20) Bozdemir, S. *Phys. Status Solidi B* **1981**, *103*, 459; *104*, 37.
(21) Skinner, J. L. *J. Chem. Phys.* **1983**, *79*, 1955; **1985**, *82*, 5232.
(22) Jernigan, R. L. In *Dielectric Properties of Polymers*; Karasz, F. E., Ed.; Plenum: New York, 1972; p 99.
(23) Flory, P. J. *Statistical Mechanics of Chain Molecules*; Interscience: New York, 1969.
(24) Monnerie, L.; Lauprêtre, F. *Structure and Dynamics of Molecular Systems* Daudel, R., Ed.; D. Reidel: Dordrecht, 1986.
(25) Bendler, J. T.; Yaris, R. *Macromolecules* **1978**, *11*, 650. Skolnick, J.; Yaris, R. *Macromolecules*, **1982**, *15*, 1041; *15*, 1046.
(26) Hyde, P. D.; Waldow, D. A.; Ediger, M. D.; Kitano, T.; Ito, K. *Macromolecules* **1986**, *19*, 2533.
(27) This matrix $\mathcal{C}^{(N)}$ is the transpose of the conventional time-dependent transition probability matrix of Markov chains, where the *ij*th element is related to the conditional passage from state *i* at epoch t to state *j* at epoch τ with $\tau > t$. See, for example: Feller, W. *An Introduction to Probability Theory and its Applications*, 3rd ed.; Wiley: New York 1971; Vol I.
(28) Abe, A.; Jernigan, R. L.; Flory, P. J. *J. Am. Chem. Soc.* **1966**, *88*, 631.
(29) See, For example: Eyring, H. *J. Chem. Phys.* **1935**, *3*, 107. Wynne-Jones, W. F. K.; Eyring, H. *Ibid.* **1935**, *3*, 492; Glasstone, S.; Laidler, K. J.; Eyring, H. *The Theory of Rate Processes*; McGraw-Hill: New York, 1941; Chapter 4.
(30) The front factor has dimensions of $(\text{length})^2/\text{time}$ according to the treatment of ref 9. Transformation to dimensions of $1/(\text{time})$, required in the present treatment, was made upon dividing by $l^2 \sin^2 \theta$, where l is the bond length and θ is the supplemental bond angle. The numerical value of γ was taken as the mean of the corresponding values of trans and gauche conformations.
(31) Viovy, J. L.; Frank, C. W.; Monnerie, L. *Macromolecules* **1985**, *18*, 2606.
(32) Blomberg, C. *Chem. Phys.* **1979**, *37*, 219.

Structure of Many-Arm Star Polymers: A Molecular Dynamics Simulation

Gary S. Grest,*†‡ Kurt Kremer,†§ and T. A. Witten†

Corporate Research Science Laboratories, Exxon Research and Engineering Company, Annandale, New Jersey 08801, Institut für Physik, Universität Mainz, D-6500 Mainz, Federal Republic of Germany, and Institut für Festkörperforschung der Kernforschungsanlage Jülich, D-5170 Jülich, Federal Republic of Germany.
Received October 20, 1986

ABSTRACT: We present a detailed simulation study of star polymers with many ($6 \le f \le 50$) arms f. Each arm consists of $N = 50$, 100, or 200 monomers. In most respects these show good agreement with the asymptotic scaling predictions of the Daoud–Cotton blob model. We report values for the universal ratios characterizing the scattering from such stars. We especially concentrate on many-arm properties and on deviations from recent scaling arguments and describe in detail anomalies in the structure factor. Because typical experimental systems have arm lengths that are on the border line to the asymptotic behavior, we expect that our results are relevant for the interpretation of experiments for both star polymers and micellar solutions.

I. Introduction

Branched polymers are important in our understanding of gels and rubber. Star polymers, one special class of branched polymers, have only recently been more intensively studied[1] following the progress of synthesizing such systems which has been made during the last few years. Star polymers are macromolecules where linear homopolymers are chemically attached to a seed or center molecule. The size of the seed is typically of the order of a bond length or somewhat larger but very small compared to the extension of the chains. Experimental stars were recently produced with up to 18 arms[2] connected to a single center. While using linear polymers with associating end groups, one can even produce starlike structures with many more arms.[3] Theoretically the main interest up to now was concentrated on the asymptotic properties of stars in the limit of very long arms of N bonds per arm where the number of arms f is fixed. Although a scaling theory[4,5] and several field theoretical approaches[6-8] exist for such systems, little is known theoretically about the scattering of such objects. The only numerical studies[5,9,11,12] of these systems have concentrated on the critical exponents and the ratio of the mean-square radius of the star polymer to that of the linear polymer.[12] They have not investigated the static and dynamic structure function. Even less is known for systems with relatively few bonds N but many arms f. For such systems scaling arguments become somewhat ambiguous, and no analytic treatment is available up to now. This regime is important in light of the recent progress in synthesizing new stars and is already relevant for the investigation of dilute micellar structures.[3] For this reason, we have carried out a numerical and scaling study of star polymers in the regime where the

†Exxon Research and Engineering Co.
‡Universität Mainz.
§Institut für Festkörperforschung der Kernforschungsanlage Jülich.

0024-9297/87/2220-1376$01.50/0

number of monomers per arm is not very large but the number of arms f is.

In the present work, we will concentrate on the static properties of such star polymers with $N = 50$, 100, or 200 bonds per arm and f arms ($6 \le f \le 50$). By the choice of these parameters we are able to cover the transition from very tenous objects ($f = 6$ and 10), which can be simulated on a lattice, up to rather dense and rigid stars ($f = 40$ and 50), which cannot be simulated on a lattice easily. In order to simulate such systems, which have strong density fluctuations, we will use molecular dynamics methods.[13] Lattice Monte Carlo only allows for a few arms, while continuum MC runs into problems when dealing with systems with such strong density fluctuations.[14]

In section 2, we describe the simulation method and the systems in detail. In section 3, we present our results and a comparison of our data with recent scaling theories, while section 4 contains a discussion of the static structure function $S(q)$. In section 5, we describe our measurements of the relaxation of a single arm in the star and section 6 contains our conclusions and proposes some experiments to test the ideas presented here.

II. Method, Model, and Systems

To simulate a star polymer with many arms, we use a molecular dynamics method in which the monomers are coupled to a heat bath.[13] Thus we solve the equations of motion

$$m\frac{d^2\mathbf{r}_i}{dt^2} = -\nabla U_i - \Gamma\frac{d\mathbf{r}}{dt} + \mathbf{W}_i(t)$$

where Γ is the bead friction, $\mathbf{W}_i(t)$ describes the random force of the heat bath acting on each monomer and U_i is the potential. $\mathbf{W}_i(t)$ is a Gaussian white noise with

$$\langle \mathbf{W}_i(t)\cdot\mathbf{W}_j(t')\rangle = \delta_{ij}\delta(t-t')6k_BT\Gamma/m$$

The Einstein relation leads to a diffusion constant for an isolated bead of $D_0 = k_BT/\Gamma$. Further technical details are explained in ref 13. Each polymer consists of a seed monomer that is connected with f linear arms. Each arm has N monomers, with one free end and one end attached to the seed monomer. We will refer to a star as f/N to characterize the number of arms and number of monomers per arm. For comparison, we will also show results for a single linear chain of 50 or 100 monomers, which we refer to as 1/50 and 2/50, respectively. All monomers interact with a short-range repulsive Lennard-Jones potential, which vanishes beyond a distance $2^{1/6}\sigma$. An additional attractive force between nearest-neighbor monomers is added along the sequence of each arm. The parameters chosen are the same as in ref 13. The time step was $\Delta t = 0.006\tau$, where $\tau = \sigma(m/\epsilon)^{1/2}$. Here σ is the unit of length, m is the unit of mass, and ϵ is the unit of energy in the Lennard-Jones potential. The reduced temperature k_BT/ϵ was 1.2. The bead friction Γ acts as coupling to the viscous background and was chosen to be $\Gamma = 0.5\tau^{-1}$. The average bond length between nearest-neighbor beads along the chain was 0.97σ. Our choice of parameters ensures that the bonds do not cut each other; this is important for future analysis of the dynamical properties of the stars.

With this method[15] we studied systems of $N = 50$ bonds per arm for $f = 6$, 10, 20, 30, 40, and 50 arms, as well as stars with $N = 100$ and 200 for $f = 10$. As we saw earlier during the test of the method for single linear and ring polymers, the single polymer chain with $N = 50$ bonds exhibits the asymptotic swelling exponent ν for the end-to-end distance and the radius of gyration within a few percent. In the scaling regime the structure function $S(q)$ is proportional to $q^{-1/\nu}$. For the isolated chain with $N = 50$ we[13] found $\nu = 0.60$, negligibly different from the best known asymptotic value $\nu = 0.588$.[16] Taking this into account, we should be able to analyze the crossover from the scaling of a star polymer to that of a micelle.

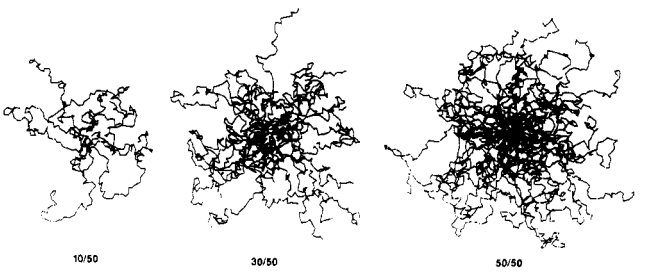

Figure 1. Projections of a typical configuration a star of $f = 10$, 30, or 50 arms with $N = 50$ monomers per arm. The pictures give an impression of the increasingly homogeneous density in the 30/50 and 50/50 systems while the 10/50 star obviously is governed much more by single-chain properties.

Special care had to be taken during the startup procedure of the simulation in order to avoid initial configurations where the monomers overlap too strongly and destabilize the simulation. First we started with the seed and connected straight lines consisting of 50 monomers with this seed. The straight parts radiated outward isotropically. The length of the bonds was set to the potential minima. Any remaining monomers were then added as a self-avoiding random walk. These starting configurations then were equilibrated over times that are much longer than the longest relaxation time of an individual arm. This time is discussed in section 5 and is shorter than that for a single polymer chain of size N. The equilibrated stars were simulated for up to 10^6 time steps. Figure 1 shows a projection of a typical configuration of a 10-, 30-, and 50-arm star with $N = 50$. The calculated quantities are described in the next section.

III. Results and Scaling Analysis

In the course of the simulation the properties were averaged over many relaxation times of a single arm. For linear chains it is known that such a dynamic simulation gives very accurate results.[13] The following quantities were calculated: The mean-square end–center distance is

$$\langle R^2\rangle = \left\langle \frac{1}{f}\sum_{i=1}^{f}(\mathbf{r}_0 - \mathbf{r}_{i,N})^2 \right\rangle \quad (1)$$

where $\mathbf{r}_{i,j}$ refers to monomer j on arm i and site $j = N$ is farthest from the center $\mathbf{r}_0$. The mean-square radius of gyration of the star is

$$\langle R_G^2\rangle = \frac{1}{Nf+1}\langle\sum(\mathbf{r} - \mathbf{r}_{cm})^2\rangle \quad (2)$$

where the sum is over all $(Nf + 1)$ monomers and $\mathbf{r}_{cm}$ is the center of gravity of the whole star molecule. We also measured the radius of gyration of each individual arm $\langle R_{Ga}^2\rangle$. In addition, the local density $\rho(r)$ as a function of distance r from the seed monomer was determined as well as several scattering functions $S(q)$, described below. In order to *analyze* our data we use the scaling ansatz of Daoud and Cotton.[4] In their picture the star consists of an inner meltlike "extended core region", an intermediate region resembling a concentrated solution, and an outer semidilute region. Since our potential has no attractive interactions, we can simplify their relations. We do not find a regime where the "Θ-blobs" are larger than the correlation length. For our model we expect to find the self-avoiding walk properties as soon as the screening length clearly exceeds the persistence length (which is

about 1.4σ bond lengths). In order to investigate this intermediate regime, we would have to include attractive interactions and study systems with much longer arms. Otherwise one cannot distinguish between the three different scaling regimes predicted by the scaling theory.[4,5] An investigation of this regime is beyond the scope of the present work. Following ref 4, we then see that for the local properties of the stars we only have to consider the "core region" and the swollen region.

For the system considered here with $f \leq 50$, we do not expect to have a very large extended core region, because $f^{1/2} < N$. Therefore it is sufficient to consider the so-called "swollen regime". The scaling results of Daoud and Cotton can then be rewritten with the dependency on the exponent ν for the special case of no attractive interactions. For ν we take $\nu_{d=3} = 0.59$.[15] Following Daoud and Cotton,[4] we find for the local swelling parameter $\alpha(r)$

$$\alpha(r) \propto f^{-1/2+1/4\nu} r^{1-1/2\nu} = f^{-0.076} r^{0.15} \tag{3a}$$

for the local screening length $\xi(r)$

$$\xi(r) \propto r f^{-1/2} \tag{3b}$$

and for the local density $\rho(r)$

$$\rho(r) \propto f^{(3\nu-1)/2\nu} r^{(1-3\nu)/\nu} = f^{0.65} r^{-1.30} \tag{3c}$$

Here r is the distance from the center of the star. Consequently one finds for the mean-square center–end distance $\langle R^2 \rangle$

$$\langle R^2 \rangle \propto N^{2\nu} f^{1-\nu} = N^{1.18} f^{0.41} \tag{4a}$$

Using $\langle R_G^2 \rangle = 1/(Nf) \int_{\sigma}^{\langle R^2 \rangle^{1/2}} r^2 \rho(r)\, d^3r$ yields

$$\langle R_G^2 \rangle \propto N^{2\nu} f^{1-\nu} \tag{4b}$$

To test whether it is sufficient to consider only the swollen regime, we first analyze the density $\rho(r)$. Figure 2a gives the density profile $\rho(r)$ vs. r for four stars with $N = 50$. In Figure 2b, we show the same data scaled as in eq 3c. In Figure 2c, we show $\rho(r)$ for $f = 10$ for $N = 50$ and 100. The slope of ln $\rho(r)$ vs. ln r is approximately 1.25, in reasonably good agreement with the expected value $(1 - 3\nu)/\nu = 1.30$. Even our most dense system ($f = 50$, $N = 50$) shows no significant deviation from the scaling form, Figure 2a. From this point of view the present systems clearly exhibit the scaling of the swollen stars and there is no need to consider in addition the core area.

This scaling also should be exhibited by the radius of gyration and the center–end distance. Figure 3 gives a log–log plot of our results for $\langle R_G^2 \rangle / \langle R_{G1}^2 \rangle$ and $\langle R^2 \rangle / \langle R_{G1}^2 \rangle$ vs. f, where $\langle R_{G1}^2 \rangle$ is the radius of gyration for a single polymer chain of N monomers. Also shown are experimental results[26] for $\langle R_G^2 \rangle / \langle R_{G1}^2 \rangle$ for polystyrene and polyisoprene. For large N, these two ratios must converge to a universal function of f that is independent of the composition of the chains. Results for $\langle R_G^2 \rangle / \langle R_{G1}^2 \rangle$ for $f = 10$ and $N = 50$, 100, and 200 indicate that by $N = 50$ this universal function of f has been attained. This viewpoint is strongly supported by the agreement with the experimental results.[27] In Table I are given the values of $\langle R_G^2 \rangle$, $\langle R_{Ga}^2 \rangle$, and $\langle R^2 \rangle$, and the number of configurations M averaged over.[17] The configurations averaged over were chosen $100\Delta t$ apart and therefore are not completely statistically independent. However from examination of the statistical fluctuations averaged over 6–10 subintervals, the data should be accurate to better than 2%. As can be seen from Table I, $\langle R_{Ga}^2 \rangle$ is only very weakly dependent on f. $\langle R_G^2 \rangle$ and $\langle R^2 \rangle$ clearly follow a power law with a slope of approximately 0.39 ± 0.03, within the error bars of the expected value of $(1 - \nu) = 0.41$. The universal ratio $\langle R_G^2 \rangle / (\langle R_{G1}^2 \rangle f^{1-\nu})$ has the value 1.55 ± 0.05 using the results with $N = 50$ and for the stars with a large number of arms $f = 30$, 40, and 50. For small f, <20, we find a significant deviation, particularly for $\langle R^2 \rangle$. One can explain this overshooting for small f by crossover effects from

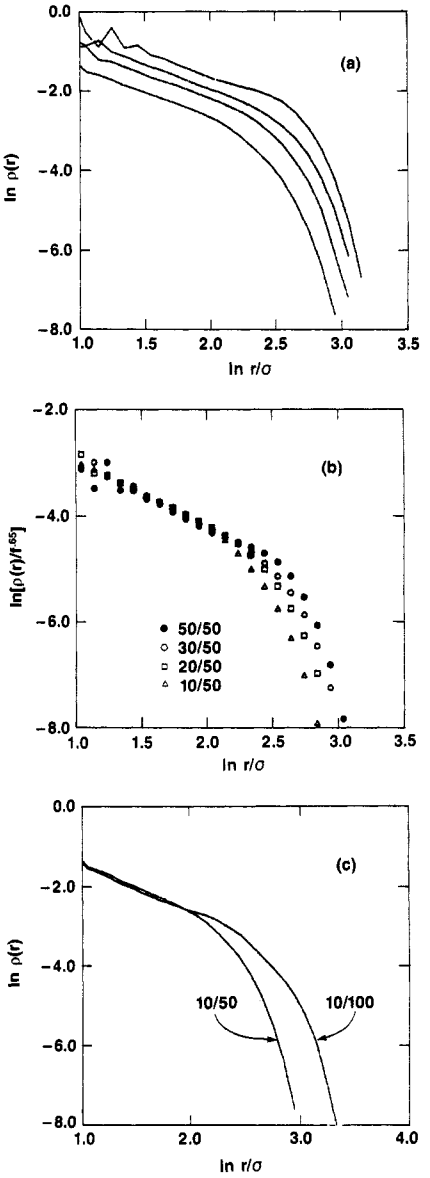

Figure 2. (a) log–log plot of density $\rho(r)$ vs. r for (top to bottom) the $f = 50$-, 30-, 20-, and 10-arm stars with $N = 50$ monomers per arm. (b) Scaling plot of $\rho(r)/f^{0.65}$ vs. r for the same four stars shown in (a). (c) log $\rho(r)$ vs. log r for two 10-arm stars with $N = 50$ and 100.

Table I
Radius of Gyration of the Entire Star $\langle R_G^2 \rangle$, Radius of Gyration of a Single Arm $\langle R_{Ga}^2 \rangle$, Mean-Square End-Center Distance $\langle R^2 \rangle$, and Ratio of $\langle R_G^2 \rangle / \langle R^2 \rangle$ for the Star Polymers Studied

f/N	M^a	$\langle R_G^2 \rangle$	$\langle R_{Ga}^2 \rangle$	$\langle R^2 \rangle$	$\langle R_G^2 \rangle / \langle R^2 \rangle$
1/50	20000	23.5			
2/50	40000	58.0			
6/50	10000	87.3	24.7	190.8	0.46
10/50	6600	102.2	25.4	207.8	0.49
20/50	3100	125.6	27.4	246.5	0.51
30/50	2600	148.1	28.6	290.6	0.51
40/50	800	163.8		321.9	0.51
50/50	1500	179.2	32.5	347.6	0.52
10/100	4500	226.9	62.5	450.5	0.50
10/200	3500	548.2	135.3	1039.7	0.53

[a] Number of configurations,[17] taken $100\Delta t$ apart, over which the quantities were averaged.

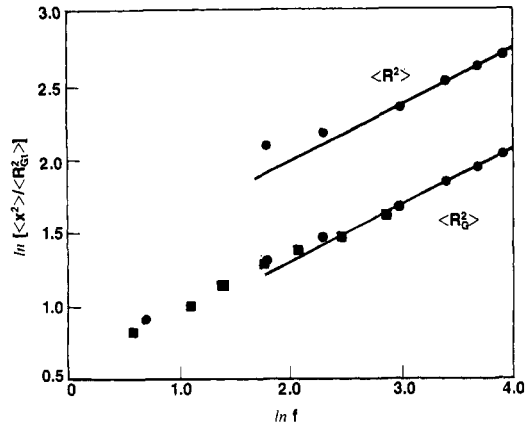

Figure 3. Radius of gyration $\langle R_G^2\rangle/\langle R_{G1}^2\rangle$ and average square end–center distance $\langle R^2\rangle/\langle R_{G1}^2\rangle$ vs. f, where $\langle R_{G1}^2\rangle$ is the radius of gyration for a single polymer chain of $N = 50$ monomers. The solid squares are data for polystyrene and polyisoprene from ref 26. The solid line indicates the predicted asymptotic power, 0.41.

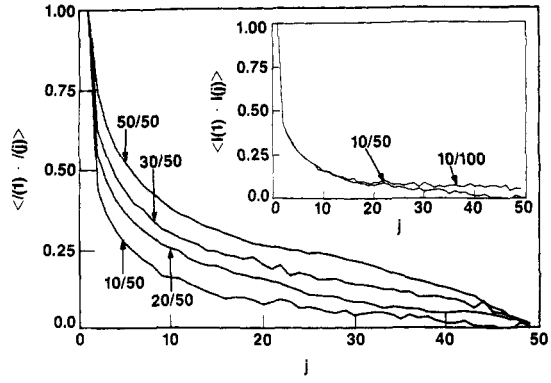

Figure 4. Bond orientation $\langle\hat{l}(1)\cdot\hat{l}(j)\rangle$ vs. j, the chemical distance from the center along the arm for $N = 50$ and $f = 10$, 20, 30, and 50. The inset shows results for $f = 10$ and $N = 50$ and 100. The two curves in the inset are identical for $j \leq 25$. Then the correlation for the $N = 50$ system breaks down, while the slow decay for the 10/100 star persists. This indicates that the internal orientational structure is independent of the length of the arm but depends strongly on f.

the $(fN)^{2\nu}$ law for $f = 1$ and 2 to the $N^{2\nu}f^{1-\nu}$ for $f \gg 1$. The intermediate range thus shows a weaker f dependence. Note that the ratio $\langle R_G^2\rangle/\langle R^2\rangle$ steadily increases for small f and is clearly larger than the value $2^{1/2}/6$ for the random walk star. This value should be in the limit of small f approximately $2^{\nu}/6$ for a self-avoiding star. The upper limit is the homogeneously filled hard sphere for which $\langle R_G^2\rangle/\langle R^2\rangle = {}^3/_5$.

The confinement produced by the other arms forces an effective stretching of the individual arm. Thus we expect a stronger correlation of bond orientations for the stars than for free chains. This can be seen from Figure 4, where we show our results for $\langle\hat{l}(1)\cdot\hat{l}(j)\rangle$ vs. j, the distance from the center of the star, where $\hat{l}(j) = (\mathbf{r}_{i,j} - \mathbf{r}_{i,j+1})/|\mathbf{r}_{i,j} - \mathbf{r}_{i,j+1}|$. As expected, the decay with distance from the center decays more slowly as f increases. For the ideal case of a chain in a cone, it is easy to estimate the decay of the bond correlation. Let the first bond define the cone axis. At a distance r from the center the diameter of the cone is given by $\xi(r)$. A blob of size $\xi(r)$ contains $\xi(r)^{1/\nu}$ monomers, which have to span the distance $\xi(r)$ along the cone axis. Thus, as long as $\xi(r) < \xi(R)$, we find that the bond correlation

$$\langle\hat{l}(0)\cdot\hat{l}(\mathbf{r})\rangle \propto (rf^{-1/2})^{(1-1/\nu)} \tag{5a}$$

which gives after inserting eq 4

$$\langle\hat{l}(1)\cdot\hat{l}(j)\rangle \propto j^{\nu-1}f^{(1-\nu)/2} \tag{5b}$$

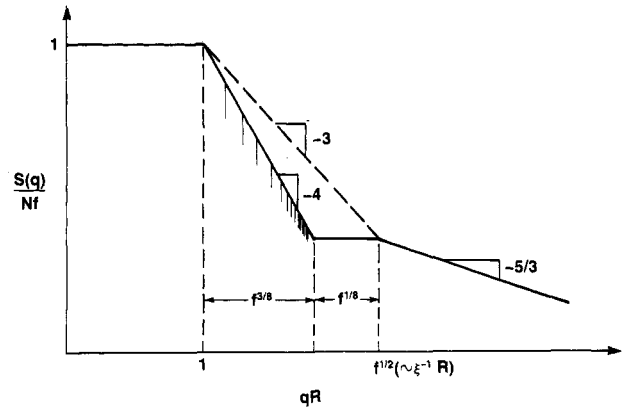

Figure 5. Schematic log–log plot of $S(q)/Nf$ vs. qR_G to show the scaling regimes for large N and f. The three characteristic lengths in the text appear as breaks in the curve. The scaling of these is indicated.

However, analysis of the data shows that the single-cone picture is not sufficient. The chains are not simply confined to a single cone. With increasing f this confinement is more nearly fulfilled. This results in an effectively larger f dependence than that predicted by eq 5b. In agreement with the predicted dependence on the chemical distance along the chain $\langle\hat{l}(1)\cdot\hat{l}(j)\rangle/j^{\nu-1}$ shows a plateau for $j < N/2$; for large f, $f = 30$ and 50. For $j > N/2$, the argument for the confinement of the succession of blobs is no longer valid. This point is clearly demonstrated in the inset of Figure 4, where we compare the bond correlation for the 10/50 and 10/100 stars.

IV. Structure Functions

The Daoud–Cotton picture of the star polymer allows us to anticipate the behavior of its structure function $S(q)$

$$S(q) = \frac{1}{(Nf+1)}|\Sigma\exp(i\mathbf{q}\cdot\mathbf{r})|^2 \tag{6}$$

where the sum is over all $(Nf + 1)$ monomers. The scaling regimes are limited by three characteristic lengths: the radius R of the star, the correlation length $\xi(R)$ of the largest blob and the monomer size σ. As noted above, $\xi(R)$ scales as $Rf^{-1/2}$. For $qR < 1$, $S(q)$ has the normal Guinier behavior: $S(q) = Nf[1 - q^2\langle R_G^2\rangle/3 + \mathcal{O}(q^4\langle R_G^2\rangle^2)]$. For $\xi(R)^{-1} < q < \sigma^{-1}$, it is convenient to understand the scattering by covering the polymer with spheres of radius q^{-1}. In the absence of strong correlations between the positions of the spheres, these scatter incoherently. The resulting scattering intensity $NfS(q)$ is the number of spheres times the average structure function for a single sphere. In the star polymer, the great majority of these imaginary spheres are contained within blobs much larger than the spheres. The contents of each sphere and the correlations between spheres are thus nearly the same as in a simple excluded volume polymer. This gives a fractal scattering law[18] $S(q) \propto q^{-1/\nu}$, independent of f and N. The only difference in the star's $S(q)$ comes from a small volume near the center, where there are blobs smaller than q^{-1}.

Between $q \simeq R^{-1}$ and $q \simeq \xi(R)^{-1}$, $S(q)$ must fall from about $Nf \simeq (\xi(R)/\sigma)^{1/\nu}(R/\xi(R))^d$ to about $(\xi(R)/\sigma)^{1/\nu}$. The limiting $S(q)$ in the Guinier ($qR < 1$) and fractal ($q\xi(R) > 1$) regimes are connected by a power law q^{-d}, as shown in Figure 5.[19]

The actual scattering for $R^{-1} < q < \xi(R)^{-1}$ does not follow this q^{-d} "envelope". In this regime, the scattered wavelength q^{-1} is larger than the largest blob, and the polymer chain structure is invisible to the scattering. $S(q)$ is essentially unaffected by moving the elementary scatterers

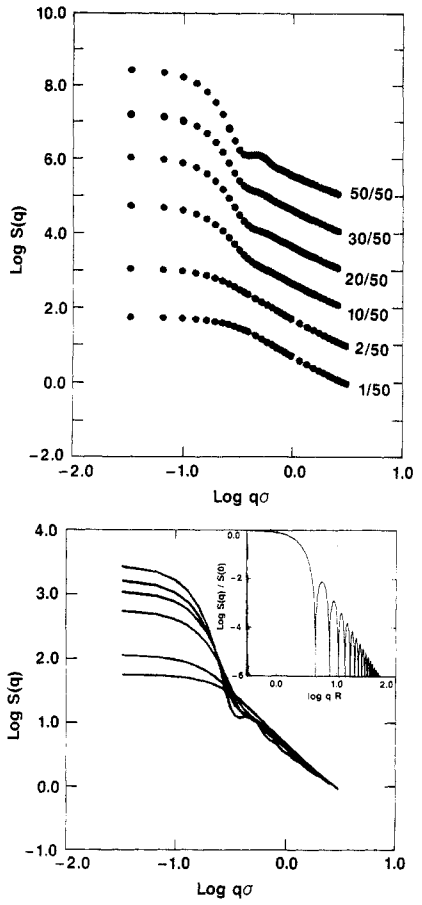

Figure 6. (a) $S(q)$ vs. $q\sigma$ for five star polymers with f = 10–50 for N = 50. Also shown are the results for two linear polymers with 50 and 100 monomers. The data has been offset for clarity. (b) Same data as in (a) plotted without offsetting to show that the results for high q lie on top of one another. Results for $S(q)/S(0)$ vs. qR for a homogeneous sphere are shown as an inset to (b).

a distance less than about q^{-1}, so that the monomers may be dispersed throughout their blobs without altering the scattering. What remains is a smooth density profile, a cloud of uncorrelated scatterers with a $r^{-(1-3\nu)/\nu}$ density profile. In the simplest Daoud–Cotton picture, the density at the outer limits of this cloud falls off with a skin depth of order $\xi(R) < q^{-1}$. The scatterers are confined in a spherical region of roughly uniform density, whose radius is well defined to $\approx\xi(R)$. Such a spherical region gives rise to the classical hard-sphere scattering pattern shown in the inset to Figure 6b. The oscillations are superimposed on a q^{-d-1} Porod envelope. Experimentally the oscillations, which depend on the radius R being the same for all polymers in the sample, would often be washed out by polydispersity effects.

This Porod scattering falls off rapidly with increasing q. Ultimately, it falls below the incoherent scattering from the Daoud–Cotton blobs. For $q < \xi(R)^{-1}$ these are expected to scatter like a semidilute solution with correlation length $\xi(R)$. Thus $S(q)$ becomes constant for $q\xi(R) < 1$: $S(q) \simeq (\xi(R)/\sigma)^{1/\nu}$. The Porod scattering becomes equal to this constant for $qR \simeq f^{d/(2(d+1))}$ or $q\xi(R) \simeq f^{-1/(2(d+1))}$. This q defines a fourth characteristic length needed to separate the scaling regimes.

We tested these predictions by computing the $S(q)$ for our simulated stars. In order to obtain good statistics 30 **q** vectors were chosen randomly from a sphere of radius $|\mathbf{q}|$ for each configuration. We averaged our results over 1000–5000 star configurations $100\Delta t$ apart. Figure 6 gives the total structure factor $S(q)$ for a star polymer with f = 10–50 for N = 50 and for two single linear polymer chains with N = 50 and 100, labeled 1/50 and 2/50, respectively. In Figure 6a, the results have been offset for clarity. In Figure 6b, we present the same data without offsetting to show that the results for high q lie on top of each other, as expected from the scaling analysis above. In this regime, the q dependence appears to approach the predicted $q^{-1/\nu}$ law; however for large f, ν seems to be larger than expected, ν = 0.65 ± 0.05. A second universal ratio $S(q) \times (q^2\langle R_G^2\rangle)^{1/2\nu} f^{3/2-1/2\nu}/S(0) = 1.4 \pm 0.4$ in this q regime if we used the correct value of ν = 0.59. In Figure 7, we present results for $S(q)$ for the 10/200 star compared to the 10/50 star.

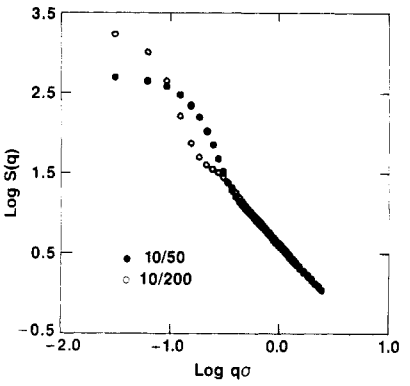

Figure 7. $S(q)$ vs. $q\sigma$ for the 10/200 and 10/50 star.

Note that as the number of arms increases, $S(q)$ becomes more structured and falls off very strongly. A "terraced" behavior is also seen for large f. The steps, as indicated by the arrows, occur at $2\pi n/\langle R^2\rangle^{1/2}$, n = 1, 2, ... For f = 50 one can find two steps. These periodic steps suggest a rather sharp cutoff in the monomer density at radius R. Indeed, if one calculates $S(q)$ of a homogeneous sphere of a given radius r one finds

$$S(q) = (4\pi)^2R^2q^{-4}\left\{-\cos qR + \frac{\sin qR}{qR}\right\}^2 \qquad (7)$$

On the average $S(q)$ shows the well-known dominant q^{-4} behavior. But the q^{-4} slope only describes the envelope of the maxima in $[-\cos x + (\sin x)/x]^2$, which approaches a periodicity of $2\pi/R$ for $x \gg 1$. This can be seen from the inset of Figure 6b, which shows a plot of eq 7. For the present systems, only for f = 50 do we see some agreement to the overall q^{-4} dependence. Similar results have not been seen experimentally because starlike polymers with f as large as we have studied here do not exist at present. However it should be possible to make such systems experimentally, especially for micellar systems. There exists already one class of systems which exhibits a similar behavior. In a recent neutron scattering experiment Richter et al.[20] measured the static structure factor of so-called "tree-like microgels" where the number of cross-links varies from 0 to 0.01 per monomer. These systems exhibit an $S(q)$ that is very similar to the one we observe. In order to explain the similarities in more detail, of course more work is needed, both from theory and experiment.

Another important question is the behavior of a single arm of the star. This can be studied by measuring the structure function $S_a(q)$ of a single arm. Figure 8 shows the single-arm scattering function $S_a(q)$ for N = 50 and f = 10–50. In Figure 9, we show $S_a(q)$ for f = 10 with N = 50 and 200. For large q all the different systems show a power law behavior. For free chains one expects a $S(q) \propto q^{1/\nu}$ behavior. The slopes of the high-q part of $S_a(q)$ in Figure 8 exhibit a power law with an effective ν of $\nu \approx 0.63$

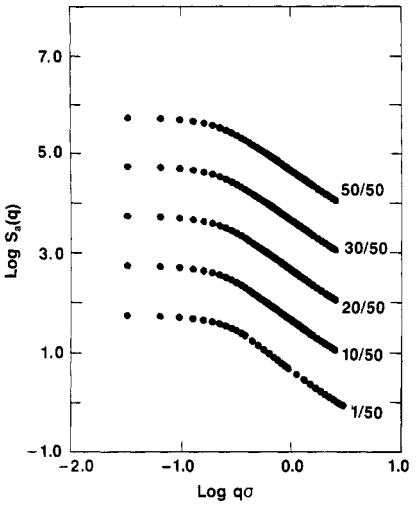

Figure 8. Single-arm scattering function $S_a(q)$ vs. $q\sigma$ for four stars with f = 10–50 and N = 50. For comparison, we have also plotted the results for a linear chain of 50 monomers (1/50).

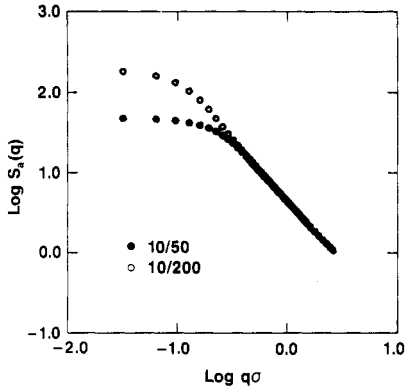

Figure 9. $S_a(q)$ vs. $q\sigma$ for the 10/200 and 10/50 stars.

for $f \geq 10$, while the high-q part of $S_a(q)$ for the 10/200 star (Figure 9) gives $\nu \approx 0.61$. As expected, as N increases, the effective value of ν approaches 0.59. This is in good agreement with the scaling behavior of the center–end distance observed in Figure 3b. But there is one difference. At larger distances a different regime is developing with increasing number of arms f. A similar effect was seen for chains confined to a straight tube.[21] The fact that the arms are effectively confined to some kind of cone can be seen even more clearly by calculating $S_a(q)$ for the inner and the outer half of a *single* arm, as seen below.

Since we have the monomer positions, it is possible to measure other structure functions in addition to the total and single-arm $S(q)$'s discussed above. This is done by labeling parts of the chain, exactly as is done experimentally by hydration or deuteration. By labeling only the inner $N/2$ or outer $N/2$ monomers of each chain, we can measure the contribution of the scattering function from the inner core regime or the outer monomers which are nearly free-chain-like. Results for the inner and outer contributions to the total structure function $S(q)$ are shown in Figure 10 for six stars. Similar results for the inner and outer components of $S_a(q)$ are shown in Figure 11.

V. Relaxation Phenomena

Our simulation gives information about the relaxation dynamics of star polymers. We will explore this subject further in a forthcoming paper. Here, we report only the simplest relaxation phenomena to show how the simulated stars approach equilibrium. We monitored the fluctuations in the end–center distance R and in the radius of gyration

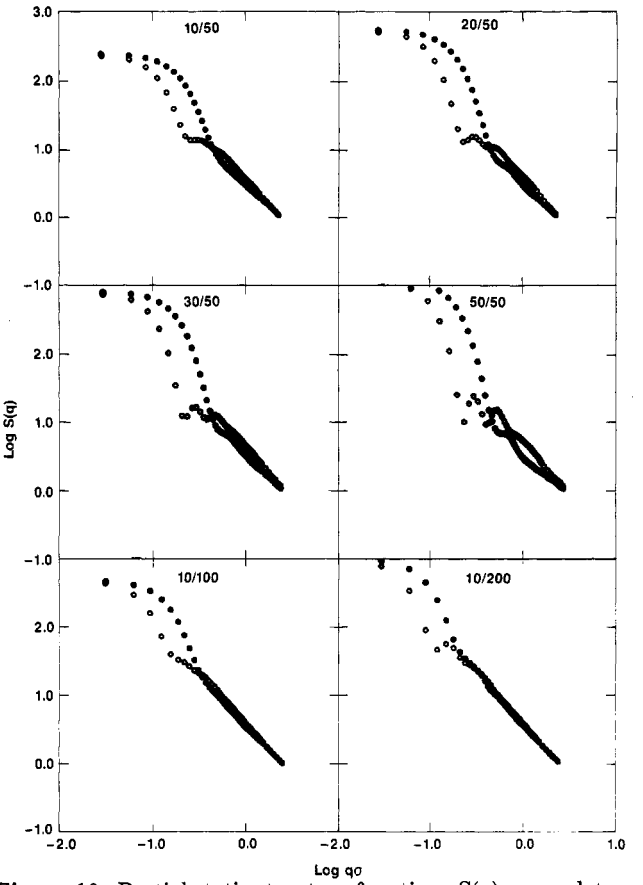

Figure 10. Partial static structure functions $S(q)$ vs. $q\sigma$ determined by scattering from only the inner $N/2$ monomers of each arm (closed circles) or from the outer $N/2$ monomers of each arm (open circles).

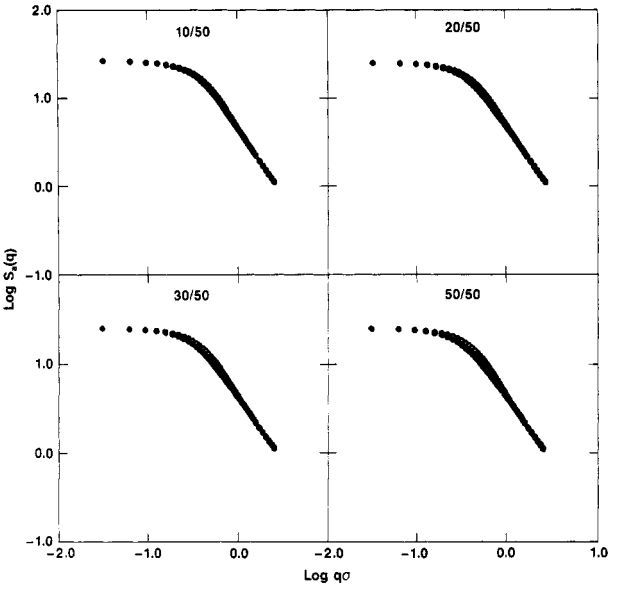

Figure 11. Partial static structure functions $S_a(q)$ vs. $q\sigma$ determined by scattering from only the inner $N/2$ monomers of a single arm (closed circles) or from the outer $N/2$ monomers of a single arm (open circles).

R_{ga} of each arm. Then we constructed the autocorrelation function $C_R(t)$ defined by

$$C_R(t) \equiv (\langle R(t)R(0)\rangle - \langle R\rangle^2)/(\langle R^2\rangle - \langle R\rangle^2) \quad (8)$$

The averages $\langle ... \rangle$ are over initial states (t = 0) taken $20\Delta t$ apart and over all f arms. Thus $C_R(t)$ decays from 1 to 0 as t goes from 0 to infinity. We measured the analogous

Table II
Relaxation time τ_R for the End-Center Distance R and Single-Arm Radius of Gyration R_{Ga} as Determined from eq 9

f/N	M^a	τ_R	$\tau_{R_{Ga}}$
6/50	20000	56.3	41.6
10/50	10000	58.0	58.8
20/50	10500	59.8	58.8
30/50	10000	66.0	67.2
50/50	6250	57.8	59.8
10/100	10000	237.4	236.7

[a] The number of initial states, chosen $20\Delta t$ apart, that $C_R(t)$ was averaged over.

function $C_R(t)$ for the radius of gyration R_{Ga}.

We may use the Daoud–Cotton[4] picture to anticipiate the behavior of $C_R(t)$. We estimate the center–end distance fluctuations by considering a single arm confined to a cone. In this system, as in a simple stretched chain,[22] the fluctuations in the total length arise from independent fluctuations of order ξ within each blob. Thus the end–end distance[23] fluctuates by an amount $\xi(R/\xi)^{1/2}$. For the star, $\xi \simeq Rf^{-1/2}$, so that we expect $(\langle R^2\rangle - \langle R\rangle^2) \simeq \langle R\rangle^2 f^{-1/2}$. We expect the relaxation of R to occur in two stages. First, local motions of the outer blob containing a given end can relax its position in a time τ_b of the same order as the relaxation time for such blobs in isolation. In our simulations, this τ_b is the Rouse time[24] for such a blob: $\tau_b \simeq \xi^2 g$. Here $g \simeq \xi^{1/\nu}$ is the average number of monomers in the blob. From the Daoud–Cotton construction, this $g \simeq Nf^{-1/2}$. Thus $\tau_b \simeq (Nf^{-1/2})^{2\nu+1} \simeq N^{2.18}f^{-1.09}$. This initial relaxation should permit relaxation over a distance of order ξ; for large f this is a small fraction of the total relaxation. Further relaxation requires concentration fluctuations to move over distances of order R. This relaxation should be diffusive, with a diffusion constant of order ξ^2/τ_b. For relaxation to occur at a scale R should thus require a time τ_R of order $\tau_b(R/\xi)^2 \simeq N^{2.18}f^{-0.09}$.

In a real star in solution, hydrodynamic interactions modify the local relaxation. The relaxation time for a blob is now a Zimm time $\tau_b = \eta/[(k_BT)\xi^3]$, where η is the viscosity of the solvent medium. Relaxation at larger scales should occur by cooperative diffusion as in a semidilute solution. The relaxation time τ_R for the star is again given by $\tau_R = \tau_b(R/\xi)^2$. Using this formula, one deduces that the relaxation of the star is on the order of $f^{1/2}$ times faster than that of a linear chain of the same radius of gyration.

For complete relaxation of the star, including topological rearrangements of the arms, a further process is required. This rearrangement would affect the relaxation of, e.g., the distance between *two* ends. But we do not expect it to affect the single-arm autocorrelations that we measured. It would be of great interest to explore the motions leading to this rearrangement.

The observed correlation functions $C_R(t)$ for the end–center distance and for the radius of gyration of a single arm are consistent with the behavior anticipated from the above discussion. Figure 12 shows that the relaxation is expontential with a characteristic time τ_R. We see no evidence for the initial time τ_b. As shown in Table II, the final relaxation time depends imperceptibly on f and is consistent with the weak $f^{-0.09}$ dependence predicted. The relaxation time τ_R can be determined either from the slope of ln $C_R(t)$ vs. t for long times or by

$$\tau_R = \int_0 C_R(t)\, dt \qquad (9)$$

We used both methods and give similar results to within 10%. Since we do not measure the complete decay of $C_R(t)$, the integration was carried out numerically only

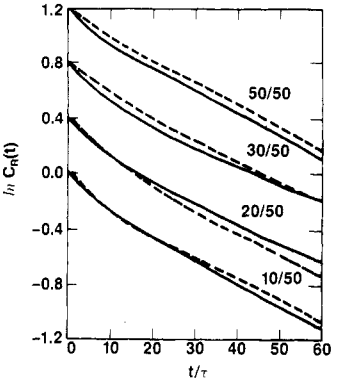

Figure 12. Autocorrelation function $C_R(t)$ for the end–center distance (solid lines) and single arm radius of gyration (dashed lines) for four stars of size 10/50, 20/50, 30/50, and 50/50. Note that the relaxation time is essentially the same for all four.

from 0 to 60τ. The contribution from 60τ to infinity was added by assuming that $C_R(t)$ decayed exponentially for long times. The same type of behavior is observed in the relaxation of the radius of gyration. As seen from Table II and Figure 12, the relaxation time τ_R is essentially the same for the end–center distance and the radius of gyration of a single arm. The N dependence of τ_R appears roughly quadratic, as anticipated. The amplitude of $\langle R^2\rangle/\langle R\rangle^2 - 1$ also shows a dependence of approximately $f^{-0.4}$, less than the predicted $f^{-1/2}$ dependence. However, we do not know if this is the asymptotic result for very large f.

In a future publication we will investigate additional relaxation processes, which might be dependent on topological rearrangements. Thus we have no evidence that our stars have relaxed topologically from their initially disentangled state.

VI. Conclusions

To conclude, we have presented a detailed numerical and analytical study of the properties of star polymers with many but relatively short arms. The arms are long enough to exhibit, as single free chains do, asymptotic behavior. By the use of a recently developed molecular dynamics technique, we were able to cover the whole area from a few arms (f = 6 and 10) up to many (f = 50) arms. Because of the strong density fluctuations standard Monte Carlo methods are *not* capable of providing data for this range of systems. It turns out that the overall properties, described by $\langle R_G^2\rangle$ and $\rho(r)$ even for the dense systems are very well described by the scaling picture.[4,5] If one looks more closely at the single arm there are deviations. $S(q)$ of a single arm indicate that the chains are more stretched than expected. This can be explained by the use of the blob picture as illustrated in ref 4. Properties such as $\langle R_G^2\rangle$ of the overall star are not affected by the question of whether an individual strand of the star is confined to its cone built by the other strands. Consequently it is not necessary that each single arm is a succession of growing blobs. The only condition for the scaling is that the overall relation f equals the number of cones is fulfilled. It will be one of the important questions during a more detailed investigation of dynamical properties whether these "fixed entanglements" are realistic and thus crucial for dynamical properties.

Another scaling property left unexplored in our study is the partition function exponent $\gamma(f)$.[25] To estimate the exponent $\gamma(f)$ one of course needs a method that counts all possible states (see, e.g., ref 11). Otherwise one finds a γ that might depend on the (numerical) history of our star polymer. Irrespectively of this discussion there are other aspects that are very important for various systems.

We think that if such stars can be synthesized, it is realistic. As mentioned in the text, recently investigated microgels[20] show qualitatively a very similar behavior. Because of their chemical structure, they have this typical cutoff in the size and $S(q)$ looks very similar to our results for large f. Another interesting check of our simulation will be possible when stars are produced with marked arms or partially marked arms. Then one should be able to reproduce all the different $S(q)$'s presented here by real experiments. Finally we want to mention that the results of Figure 10 should be reproducible not only by block copolymer stars but also by small micelles. If we take the 50/50 star this would correspond to a flexible shell of a flexible sphere, built by the 50 small chains, each consisting of $N = 50$ monomers.

The present investigation gives an intriguing first impression on the problems and properties of many-arm star polymers and related chemical systems such as treelike microgels. We hope that our results will lead to both new theoretical and experimental studies in this very interesting field of polymer science.

Acknowledgment. We thank D. Richter for communicating the results of ref 20 and L. J. Fetters for allowing us to use his unpublished data[26] in Figure 3. We thank S. Milner for considerable help in interpreting our results. We also thank M. Cates, W. Dozier, L. J. Fetters, W. Graessley, J. Huang, and D. Richter for many helpful discussions. G.S.G. thanks FFB41 for funding his visit at the Universität Mainz.

References and Notes

(1) Burchard, W. *Adv. Polym. Sci.* **1983**, *48*, 1. This paper gives an extensive review of the scattering properties of branched polymers and gives a rather complete list of references. More recent experimental papers for stars are: Roovers, J.; Hadjichristidis, N.; Fetters, L. J. *Macromolecules* **1983**, *16*, 214. Huber, K.; Burchard, W.; Fetters, L. J. *Macromolecules* **1984**, *17*, 541. Xuexin, C.; Zhongde, X.; von Meerwall, E.; Seung, N.; Hadjichristidis, N.; Fetters, L. J. *Macromolecules* **1984**, *17*, 1343. Richter, D.; Ewen, B.; Nerger, K. H.; Stühn, B., to be published.
(2) Dozier, W.; Huang, J.; Fetters, L. J., in preparation.
(3) Fetters, L. J.; Funk, W. G.; Hadjichristidis, N.; Davidson, N.; Graessley, W. W., to be published. Pearson, D. S.; Younghouse, L. B.; Fetters, L. J.; Hadjichristidis, N.; Graessley, W. W., to be published.
(4) Daoud, M.; Cotton, J. P. *J. Phys. (Les Ulis, Fr.)* **1982**, *43*, 531.
(5) Birshtein, T. M.; Zhulina, E. B. *Polymer* **1984**, *25*, 1453. Birshtein, T. M.; Zhulina, E. B.; Borisov, O. V. *Polymer* **1986**, *27*, 1078 use a slightly different ansatz than ref 4 but find the same results.
(6) Miyake, A.; Freed, K. F. *Macromolecules* **1983**, *16*, 1228; **1984**, *17*, 678.
(7) Douglas, J. F.; Freed, J. F. *Macromolecules* **1984**, *17*, 1854.
(8) Vlahos, C. H.; Kosmas, M. K. *Polymer* **1984**, *25*, 1607.
(9) Mazur, J.; McCrackin, F. *Macromolecules* **1977**, *10*, 326.
(10) Kolinski, A.; Sikorski, J. A. *Polym. Sci., Polym. Chem. Ed.* **1982**, *20*, 3147.
(11) Lipson, J. E. G.; Whittington, S. G.; Wilkinson, M. K.; Martin, J. L.; Gaunt, D. S. *J. Phys. A: Math. Gen.* **1985**, *18*, L469. Wilkinson, M. K.; Gaunt, D. S.; Lipson, J. E. G.; Whittington, S. G. *J. Phys. A: Math. Gen.* **1986**, *19*, 789.
(12) Freire, J. J.; Pla, J.; Rey, A.; Prats, R. *Macromolecules* **1986**, *19*, 452.
(13) Grest, G. S.; Kremer, K. *Phys. Rev. A* **1986**, *33*, 3628.
(14) See, e.g.: Baumgärtner, A. In *Applications of the Monte Carlo Method in Statistical Physics*; Binder, K., Ed.; Springer: Berlin, 1984; Chapter 4.
(15) For the 50/50 star, the computer program took 3 h of computer time on a Cray XMP for 100 000 time steps without the structure functions. The calculations of the structure functions required an additional 25% in computer time.
(16) Le Guillou, J. C.; Zinn-Justin, *Phys. Rev. B* **1980** *21*, 3976. In the present paper, we use $\nu = 0.59$.
(17) The single-arm radius of gyration $\langle R_{Ga}^2 \rangle$ was averaged over only about half as many configurations M as $\langle R_G^2 \rangle$ for $f \geq 10$, since this piece of analysis was added to the computer codes after some runs had already been made. However since for each star configuration, there are f contributions to $\langle R_{Ga}^2 \rangle$, the results should also be good to better than 2%.
(18) Edwards, S. F. *Proc. Phys. Soc., London* **1985**, *93*, 605. Cotton, J. P.; Decker, D.; Farnoux, B.; Jannik, G.; Ober, R.; Picot, C. *Phys. Rev. Lett.* **1974**, *32*, 1179.
(19) This q^{-d} "envelope" occurs more generally for loose assemblies of matter, in which subunits of size $\xi(R)$ are packed into larger units of size R with the same average density as the subunits. If the subunits are not packed too tightly so that strong correlations are avoided, these scatter incoherently at large q. But the assembly scatters coherently at small q. The result is a reduction in $S(q)$ by a factor $(\xi(r)/R)^{-d}$ between $q \simeq R^{-1}$ and $q \simeq \xi(R)^{-1}$.
(20) Richter, D.; Ewen, B.; Nerger, D. K. H., in preparation.
(21) Kremer, K.; Binder, K. *J. Chem. Phys.* **1984**, *81*, 6381.
(22) Pincus, P. *Macromolecules* **1976**, *9*, 386.
(23) This estimate also applies to polymers grafted to a surface, see: Milner, S.; Witten, T. A.; Pincus, P., to be published.
(24) Rouse, P. E. *J. Chem. Phys.* **1953**, *2*, 1273. de Gennes, P.-G. *Scaling Concepts in Polymer Physics*; Cornell University Press: Ithaca, NY, 1979.
(25) Witten, T. A.; Pincus, P. A. *Macromolecules* **1986**, *19*, 2509.
(26) Khasat, N.; Pennisi, R. W.; Hadjichristidis, N.; Fetters, L. J., to be published.